Energy Reports 15 (2026) 108878

Contents lists available at ScienceDirect

Energy Reports

journal homepage: www.elsevier.com/locate/egyr

Research paper

Magnetorheological elastomers: Experimental characterization and dependences of the inverse effect

Guido Napolitano Dell'Annunziata *, Renato Brancati, Giandomenico Di Massa, Andrea Genovese

Department of Industrial Engineering, University of Naples Federico II, Via Claudio, 21, Naples, 80125, Italy

ARTICLE INFO

Keywords:
Smart materials
Magnetorheological elastomers
Experimental testing
Magnetorheological inverse effect
Energy harvesting
Pseudo-villari effect

ABSTRACT

Despite the growing interest in magnetorheological elastomers (MREs), a comprehensive understanding of their inverse effect continues to be lacking, hindering the full exploitation of these materials for sensing and energy harvesting applications. In this work, we present a systematic and extensive experimental study aimed at elucidating the influence of composition, fabrication processes, and geometrical features on the inverse magnetorheological response of MREs. New insights into the functional dependencies are provided, advancing current knowledge on the mechanisms governing the behavior of these materials under mechanical stimuli. These findings establish an engineering basis for the informed design and optimization of MRE-based devices, offering useful strategies for their effective realization depending on the intended application in emerging technological fields where large deformations at low frequencies are present.

1. Introduction

In the past two decades, research and technology have put a lot of effort into developing and synthesizing active smart materials (Bahl et al., 2020; Schwartz, 2002). These materials, which can convert one form of energy (such as thermal, electrical, chemical, mechanical, or optical) into another form, have a great impact on several aspects of technology and daily life. An example of these are piezoelectric materials, shape memory alloys and electro-rheostat materials which can generate an electric charge when subjected to external strain (Yang et al., 2017; Mahapatra et al., 2021). Conventionally, when electrical energy is transformed into another form (e.g. mechanical), this behavior is referred to as "direct-effect"; the opposite conversion is named "inverse-effect". The direct effect deals with applications such as actuators or active controls of the systems (Lin et al., 2025; Zhao et al., 2024), while the inverse effect is used for sensing/monitoring and energy harvesting. Therefore, it is evident how the development and use of these types of materials involve various aspects of technology, including materials engineering, chemistry, electronics, and mechanics. The exploitation of the inverse-effect, which has a transversal impact in several fields such as industrial, civil and medical (Sobczyk et al., 2022; Zheng et al., 2021) has been growing steadily in recent years for two main interconnected reasons: the energy crisis and the need for data collection. Smart materials used as sensors are adopted for typical applications such as remote sensing, MEMS devices, portable electronics, biomedicine, structural health monitoring and early detection and protection against seismic events.

As concerns energy efficiency, this pivotal topic pushes the use of smart materials that are designed to preserve energy (Cansiz et al., 2019; Nicolay et al., 2023). This challenge has led to the innovation of advanced materials, described in Table 1, able to capture and utilize renewable or otherwise wasted energy efficiently. However, two main limits arise for the inverse-effect of nowadays used materials: (1) Their operational range is restricted to small deformations (less than 10%) and high frequencies to be effective (Ahmad et al., 2021; Liang et al., 2021); (2) the high costs and limited reusability of these materials cast doubt on their overall advantages. Another very promising technology is represented by triboelectric nanogenerators (TENGs). However, Zhang (2023) demonstrated that TENGs are irreplaceable and highly efficient for harvesting low-frequency, small-amplitude, and low-force mechanical energy, making them complementary to piezoelectric. Moreover, from a practical perspective, triboelectric nanogenerators face several limitations, including low output current, degradation due to repeated contact and friction, and strong sensitivity to environmental factors such as humidity, temperature variations, and surface contamination (Trinh and Chung, 2023).

Therefore, there is a growing need to bridge the engineering gap in smart materials for low-frequency and high-deformation applica-

* Corresponding author.
E-mail address: guido.napolitanodellannunziata@unina.it (G. Napolitano Dell'Annunziata).

https://doi.org/10.1016/j.egyr.2025.12.015
Received 21 July 2025; Received in revised form 9 November 2025; Accepted 4 December 2025
Available online 16 December 2025

Table 1
Range of use of smart materials for sensing and harvesting (Sobczyk et al., 2022).

Smart material	Young's modulus	Strain (%)	Frequency
Piezoelectrics	60–93 GPa	0.2	<1 MHz
Electrostrictives	0.4 GPa	0.1	<10 kHz
Piezopolymers	3.2 GPa	10	<100 kHz
Magnetostrictives	25–35 GPa	0.2	About 1 MHz
Shape memory alloys	25–80 GPa	4–8	<10 kHz

tions (Bellelli et al., 2025).

This wide range of applications involves the use of elastomers, providing a unique opportunity to leverage the broad and increasing adoption of such materials and enhance global energy efficiency. In this context, a new class of smart soft materials, called magneto-rheological elastomers (MREs) (Jaafar et al., 2021; Díez et al., 2021), and the corresponding technology for energy harvesting and advanced sensing/monitoring applications become more and more attractive (Costi et al., 2024; Wang et al., 2009; Diguet et al., 2020a). The motivation behind this is that elastomers have gained increasing prevalence in diverse sectors, including automotive, industrial, and civil engineering (Li et al., 2025; Ding et al., 2024). Nonetheless, owing to their inherent characteristics, the lifecycle of components made from these materials is relatively short, resulting in an urgent issue related to their disposal. As a result, the full potential of elastomers is not realized in their current use, which contradicts their expanding use, the global demand for enhanced energy efficiency, and the environmental challenges at hand. Smart elastomers represent an emerging potential technology that addresses a broad spectrum of previously unexplored application areas. Although some studies provide very useful evidences into the potential of such materials for exploiting the inverse effect (Brancati et al., 2023; Diguet et al., 2020b; Šimić et al., 2023), many dependencies of the multi-physical phenomena remain largely unexplored. In particular, Diguet et al. focus their attention on the effects of the applied shear strain, the applied magnetic field, and the filling factor (Diguet et al., 2020a,b). In Šimić et al. (2023), in addition to the filling factor and the chemical composition of the elastomers, attention is also given to the frequency dependence, although only three cases have been explored.

This paper develops a detailed methodology for the experimental analysis of MREs to explore their potential for sensing and energy harvesting applications. The focus is on identifying and analyzing the principal multi-physical dependencies associated with this material, studying the effect of the volume percentage of the magnetic particles and their orientation and, for the first time with a systematic approach, the effect of the specimens' shape and the solicitation frequency. This work also focuses on the effect of the search coil on the output voltage and highlights the existence of an optimal magnetic field, which varies depending on the specimen used. This effort aims to establish a comprehensive knowledge base that can be leveraged for the modeling and design of components manufactured using MREs. The study seeks to enable a more informed and efficient approach to both theoretical and practical advancements in this field, through the proposed systematic approach. Additionally, the findings are intended to bridge knowledge gaps, facilitating the development of optimized designs and innovative solutions across diverse engineering and scientific contexts.

2. Methodology — experimental setup & data processing

MREs have a magnetostrictive behavior so they can be used to convert mechanical energy into electrical energy. The constitutive equations of a magnetostrictive material are described in of the IEEE (1991) and reported in Eqs. (1) and (2),

$$\varepsilon = \frac{1}{G}\tau + dH \tag{1}$$

$$B = d\tau + \mu H \tag{2}$$

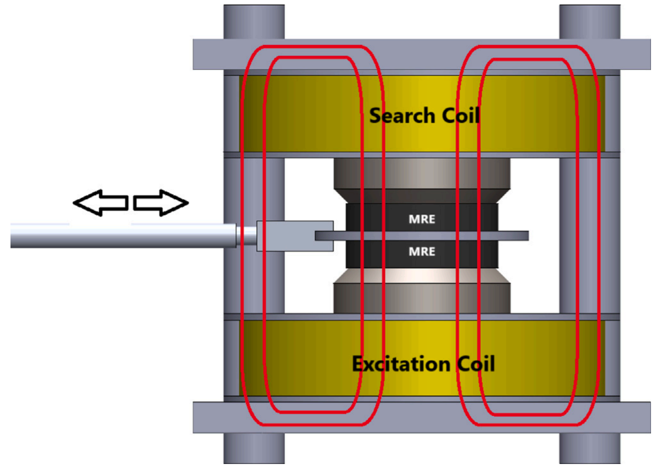

Fig. 1. Magnetic circuit scheme.

where d is the piezomagnetic constant, G is the elastic transverse modulus, μ is the magnetic permeability, H is the magnetic field, τ is the stress, B is the flux density and ε is the strain. For the MREs, the elastic modulus, the permeability and the characteristic constant varying with the strain and the magnetic flux. Thanks to this consideration, it is possible to rewrite Eqs. (1) and (2) (Deng and Dapino, 2017),

$$\varepsilon = \frac{1}{G(\varepsilon, B)}\tau + d(\varepsilon, B) \tag{3}$$

$$B = d(\varepsilon, B)\tau + \mu(\varepsilon, B)H. \tag{4}$$

If a variable strain is imposed a variable flux density is obtained, so an electrical voltage is generated on a coil, according to Faraday's law (Eq. (5)),

$$V = -N_s A \frac{dB}{dt} \tag{5}$$

where N_s is the number of turns and A is the area of the cross-section of the coil.

To evaluate the electro-mechanical behavior of magnetorheological rubbers several tests were performed employing a test rig. The experimental campaign involved four different types of MRE pads and two different kind of search coils. The magnetic circuit inside which the MRE pads were inserted is shown in Fig. 1. By means of an electromagnetic shaker, a shear strain is induced while a displacement laser sensor provides the measure of the strain. A Yokogawa acquisition instrument completes the test rig.

2.1. MRE material composition

The used elastomer is a compound of three elements: rubber matrix, catalyst, iron powder (Nugroho, 2024). A silicone rubber (Prochima GLS-10) was chosen as the matrix. To obtain low shear stiffness in order to induce large deformations, a low hardness value material is used (10 shore-A). Vulcanization occurs as a result of a polycondensation reaction obtained, at room temperature, by adding a catalyst in a 100/5 mass ratio. The Metalpolveri FE CARB was used as powder, it is composed by micro-particles (4–6 μm) of ferro carbonyl. Two different compounds were prepared with 25% and 40% in percentage volume of powder, respectively. The correct volume percentage has been obtained by weighing the components and assuming the density of the iron particles equal to 7.9 g/cm3 and of the elastomeric base component equal to 1.08 g /cm3. The components quantity are reported in Table 2.

After being mixed, the three components are placed in a vacuum chamber (between 30 and 50 mbar) for 15 min. Finally, after degassing,

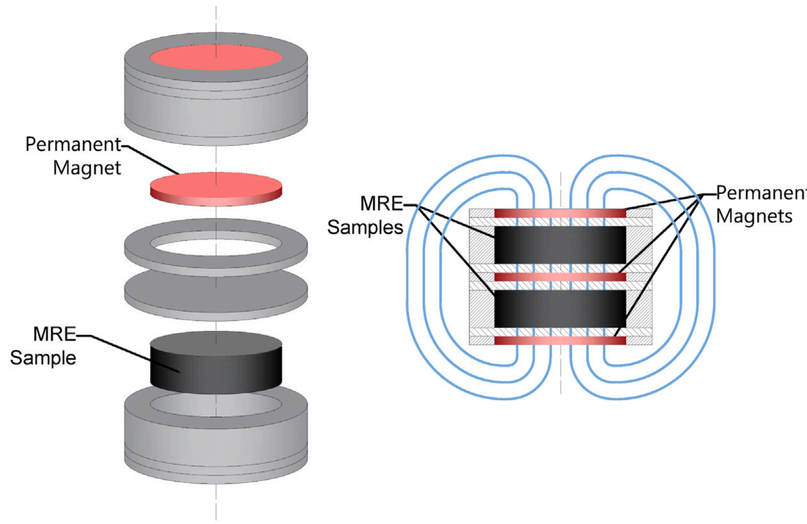

Fig. 2. MREs samples mold.

Table 2
Components quantity.

Powder %	Powder mass (g)	Rubber base (g)	Rubber catalyst (g)	Volume (cm^3)
25	118.5	46.3	2.3	60
40	189.6	37.0	1.9	60

the mixture was poured into a cylindrical mold which allowed the realization of both isotropic and anisotropic pads.

Indeed a magnetic field in the curing phase causes the iron particles to align along the field lines, therefore parallel columns of iron powder are created inside the rubber matrix. To obtain anisotropic magnetorheological rubber two permanent neodymium magnets, characterized by a maximum energy product of 263–287 kJ/m3, have been applied to the two bases of the mold (Fig. 2). Only for the compound with 25% of iron, without the permanent magnets, isotropic MRE rubber was obtained.

2.2. MRE pads properties

Four different kind of specimens were realized, differing from each other in terms of: height, iron powder percentage and isotropy. All specimens are cylindrical, with a section radius of 30 mm. The diameter was kept constant in order not to alter the housing configuration of the pads within the ferromagnetic circuit. To produce specimens with different volumes, only the pad height was varied, thus relating any difference in properties to a single geometric parameter. The choice of the two heights, 30 mm and 9 mm, stems from the intention to obtain specimens with sufficiently different volumes (a 70% reduction in volume for the 9 mm specimen compared to the 30 mm one) in order to highlight possible differences in behavior, as will be discussed in Section 3.6.

As for the iron powder percentage, two values were selected: 25%, which is commonly used as an optimal reference standard in the literature (Diguet et al., 2020b; Sebald et al., 2017), and 40%, a value rarely explored in previous works, to allow a comparison between two sufficiently distinct conditions without compromising pads functionality (higher powder contents would make the pads excessively stiff).

The fabrication of the four different types of pads, reported in Table 3 together with their main properties, was conceived to enable pairwise comparisons between pads differing in only one characteristic, as will be shown in Section 3.

Table 3
MRE pads properties.

Height (mm)	Iron powder percentage %	Isotropic/Anisotropic
9	25	Anisotropic
9	40	Anisotropic
30	25	Anisotropic
30	25	Isotropic

2.3. Magnetic circuit

The magnetic circuit is composed by the following elements:

- The excitation coil whose purpose is to generate the magnetic field. The coil is cylindrical with 1000 turns winding and 25 mm height, 60 mm inner diameter, 113 mm external diameter;
- The "Search Coil" whose purpose is to generate the output tension. Two different coils were used in the experimental campaign, with 1000 turns and 5000 turns respectively. Both are 25 mm in height, have an internal diameter of 60 mm and an external diameter of 113 mm;
- Two MRE specimens;
- Two iron plates and four iron columns.

By means of the supply current of the excitation coil, provided by a laboratory power-supply, the magnetic field is generated. In order to measure the magnetic field the magnetometer "Hirst Magnetics GM08" is used. Fig. 3 shows the four sections in which the probe was positioned.

In Figs. 4(a) and 4(b) the measured magnetic field is shown as a function of the supply current for two different types of samples, the 30 mm high specimens, oriented and not oriented, respectively. Among the four positions of the probe, the authors decided to use as a reference position 2, as it is more representative of the magnetic field that actually passes through the specimen under different test conditions. After this consideration, all the magnetic field values reported in the graphs are considered to be detected in position 2. In addition, the results will be shown with respect to the magnetic field since there is a unique correlation with the supply current for each typology of the specimens, which is deductible from Fig. 5.

In all positions and for all specimens, magnetic saturation is reached when the coil is powered with a current of approximately 6 A. Comparing the magnetic field values reached for the different specimens,

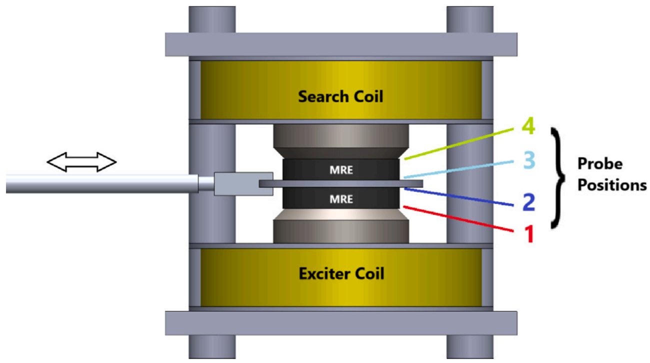

Fig. 3. Magnetic field measurement positions.

the highest field value is obtained for the lowest specimens, as is highlighted in Fig. 5 in which is shown a comparison of the magnetic field, as a function of the supply current, between the 30 mm height pads (oriented and not oriented) and the 9 mm height pads (25% CIP and 40% CIP). Fig. 6 shows the difference in height between the specimens.

The high variation in magnetic field values between specimens of different heights is due to the fact that the specimens themselves, with their geometric characteristics, modify the magnetic circuit, varying the value of the magnetic field that passes through them. Finally, it is important to report that in a real application of these MREs, such as the energy harvesting described in the Introduction, the magnetic field would be generated by permanent magnets able to exert a magnetic field suitable both for the specimen considered and for the specific application. In this scenario, the results reported in the following section constitute a fundamental step also for the determination of the optimal conditions of use and, consequently, for the choice of other components necessary for the use in the field; the one described in this paragraph is the experimental setup chosen for the study of the properties of these elastomeric materials and should not be considered as directly usable in real applications. In sensor application scenarios, it should also be possible to embed permanent magnets within elastomers by incorporating them during the vulcanization process. This approach would reduce the complexity of the ferromagnetic circuit but presents several technological challenges related to the proper sizing of the permanent magnets and the manufacturing of the pads, which certainly deserve a dedicated study.

2.4. Motion excitation system and measurement devices

In Fig. 7 in addition to the magnetic circuit, it is shown also the excitation and measurement systems. By means of the electromagnetic shaker "Bruel & Kjaer 4808", a desired motion is imposed to the MRE specimen. An appropriate tension waveform is generated by the signal generator "Tektronix AFG3022B", this tension is the input of the amplifier "SignalForce DSA1-2K" whose output is the supply of the shaker.

The voltage across the search coil winding is measured directly with Yokogawa data acquisition device.[1] The displacement is measured by means of the laser sensor OptoNCDT 1420[2] and the applied force is measured by means of the load cell Dytran 6210s[3]

[1] ADC 12 bit $\pm 1\,V$, Quantization uncertainty: $\pm 141\,\mu V$.

[2] Sensibility: $80\,\mu V/mm$; Linearity error: $\pm 40\,\mu$m; Repeatability of $2\,\mu$m; ADC 12 bit $0-5\,V$. The combined uncertainty: $u_c = \sqrt{u_{lin}^2 + u_{rep}^2 + u_{ADC}^2} = \pm 27.75$ μm.

[3] Sensibility: $5.618 mV/N$; Linearity error: $\pm 9N$; ADC 12 bit $\pm 5V$. The combined uncertainty: $u_c = \sqrt{u_{lin}^2 + u_{ADC}^2} = \pm 5.200\,N$.

The measured displacement is shown in Fig. 8. The measured output voltage is sinusoidal with double the frequency of the displacement. The acquired signal is quite noisy, therefore it was fitted with a sinusoid that better approximated it. Fig. 9 shows the measured output voltage and the fitted one. In addition, Fig. 9 presents also an RMS value of the fitted sine amplitude. In the results reported in the following sections, the RMS value of the output voltage will be used instead of the amplitude of the same signal, for its ease of comparison with other voltage quantities and power-related considerations. The value of RMS reported is obtained as the mean value of the RMS value obtained for three identical tests under the same testing conditions, this choice is made to highlight the repeatability of the tests, mitigating the small variations related to the noise of the output signal and the subsequent fitting procedure.

3. Results and investigation

3.1. Overview

This section aims to highlight all the relevant results obtained thanks to the experimental campaign carried out on the different MRE specimens. The comparison among several specimens and test conditions has been performed using as main indicator the RMS output voltage, but in some cases, other considerations can be made using other relevant KPIs such as the strain percentage, the optimal magnetic field and the solicitation frequency. Thanks to the comparisons presented below, it will be possible to highlight the variations in terms of inverse MR effect as a function of the geometric dimensions of the specimens, the content of ferromagnetic particles and their orientation, and the excitation frequency. This leads to the possibility of having a more complete picture, compared to the current state of the literature, of the strategy to be adopted for the creation of magnetorheological elastomers for energy harvesting purposes depending on the different operating conditions.

3.2. Search coil dependence

Since the final application of these elastomeric materials is energy harvesting, downstream of the ferromagnetic circuit, it is necessary to place a coil capable of reading the minimum acceptable voltage values for this kind of employment (Carlson et al., 2010). Indeed, the first set of measurements was conducted to investigate the effect that two different search coils had on the output voltage value. In particular, the two search coils adopted have 1000 turns and 5000 turns. For each configuration, the same tests have been carried out on a specimen of 30 mm height, with 25% of Carbonyl Iron Particles (CIP) oriented and with a sinusoidal imposed displacement amplitude of 1.5 mm. The experiments have been performed at six different displacement frequencies (1 Hz, 3 Hz, 5 Hz, 7 Hz, 9 Hz and 11 Hz). Different current levels in the excitation coil have been imposed for each frequency, starting from 1 A to 8 A, with an interval of 1 A among the tests. As it is possible to see in detail in the subsection focused on the magnetic circuit, it has been observed that between 6 and 7 A the corresponding magnetic field induced in the magneto-rheological elastomer saturate, as will be discussed and shown in detail in the next paragraphs. To synthesize the differences due to the different search coils, Fig. 10(a) shows the RMS output voltage amplitude for different selected magnetic field values for a fixed displacement frequency of 3 Hz. The bar plot highlights that the search coil with 1000 turns generates an output voltage an order of magnitude lower than that with 5000 turns. Both configurations exhibit an increasing voltage value with the magnetic field, reaching a maximum voltage for a specific value of the magnetic field (approximately around 200 mT) followed by a decrease in the output quantity. This behavior will be explored in detail in the subsection dedicated to the optimal magnetic field.

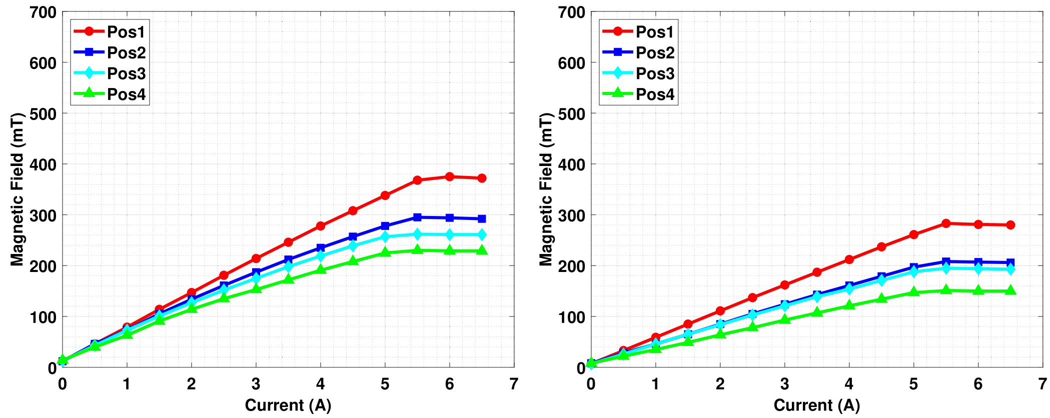

(a) 30 mm - 25% CIP - Oriented (b) 30 mm - 25% CIP - Not Oriented

Fig. 4. Current VS magnetic field.

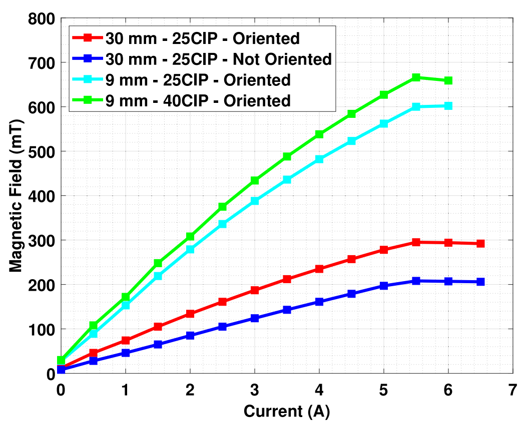

Fig. 5. Current vs magnetic field — Comparison among the specimen in Position 2.

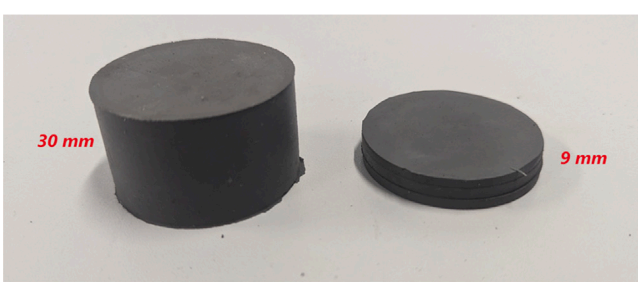

Fig. 6. MREs specimens.

The same order of magnitude difference in the output voltage is also observed in Fig. 10(b), in which the frequency effect for a fixed value of the magnetic field of 200 mT is explored. Thanks to this graph, it is also possible to affirm that increasing voltage values appear as the frequency of the displacement imposed on the specimen increases. Also this phenomenon will be deepened in the subsection focused on the frequency effect.

Due to the significant differences in the output voltage values, it was chosen to adopt the search coil with 5000 turns for all the other tests which will be described in the following paragraphs to more effectively highlight the differences among the specimens related to their different characteristics and testing conditions. Because of the higher values of output RMS voltage, it will be possible to easily identify specific behaviors and trends.

3.3. Oriented VS not oriented

Once the optimal electromagnetic configuration has been defined according to the tests described in the previous paragraph, it has been possible to start the investigation of the results of the experimental test campaign carried out. In particular, great attention was paid to the different behavior between specimens with oriented and not oriented carbonyl iron particles, referring to the 30 mm high specimen. Both the specimens have been tested with an imposed displacement amplitude of 1.5 mm, for several excitation currents from 1 A to 6 A; the tests have been repeated with increasing solicitation frequencies.

To highlight the different behaviors the RMS of the output voltage amplitude has been plotted against the measured magnetic field (Fig. 11(a)).

As it is possible to observe from the graph, the dependence between the magnetic field and the RMS output voltage seems to have a quadratic form.

The fitted curves have been truncated in correspondence with the saturation values of the magnetic field detected; this is the first main difference between the two specimens: indeed, the one with the not-oriented particles presents a magnetic field saturation value of 207 mT (vertical blue line in Fig. 11(a)) whereas for the one with oriented particles is of 294 mT (vertical red line).

As expected from the literature (Jolly et al., 1996; Lallart et al., 2017), for what concerns the output voltage the oriented specimen presents higher values than the not-oriented one. This is confirmed also for all the frequencies tested (Figs. 11(b) and 11(c)).

Also the frequency effect has been investigated: the output voltage value grows less than proportionally as the frequency increases, as can be deduced from Fig. 11(d). It is possible to state that this behavior is more evident for the oriented specimen, probably due to the higher values of output voltage reached. Looking at the trend of the output voltages described by the quadratic equations, it is possible to hypothesize that there is a saturation value of the output voltage, not explored in the study reported in this paper, but which will be the subject of subsequent analyses.

3.4. Magnetic particles' volume percentage

During the test specimens realization, regarding the 9 mm high elastomers, two different carbonyl iron percentages have been selected in order to investigate the effect of the amount of this particles. In particular, the first specimen was realized with a 25% of CIP, a value commonly used in MREs preparation that exhibits the best performance for what concerns MR direct effect (Diguet et al., 2020a), whereas the second one presents the 40% of CIP. Both specimens have been

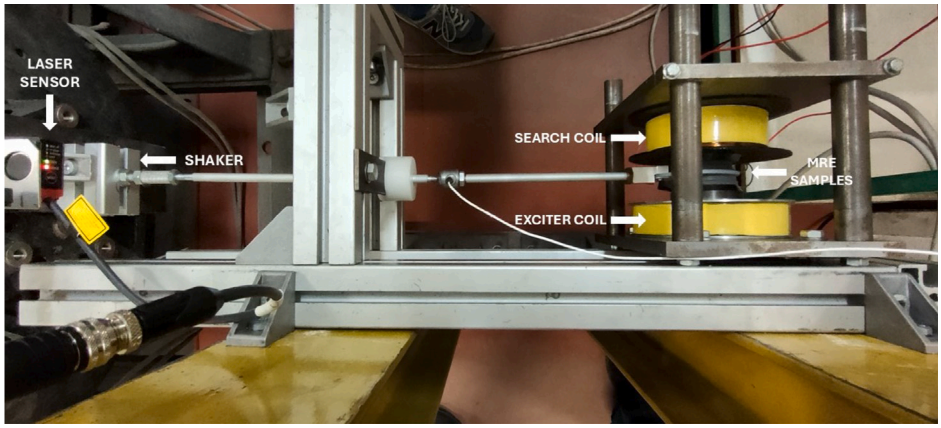

(a) Photograph of the Experimental Test Rig

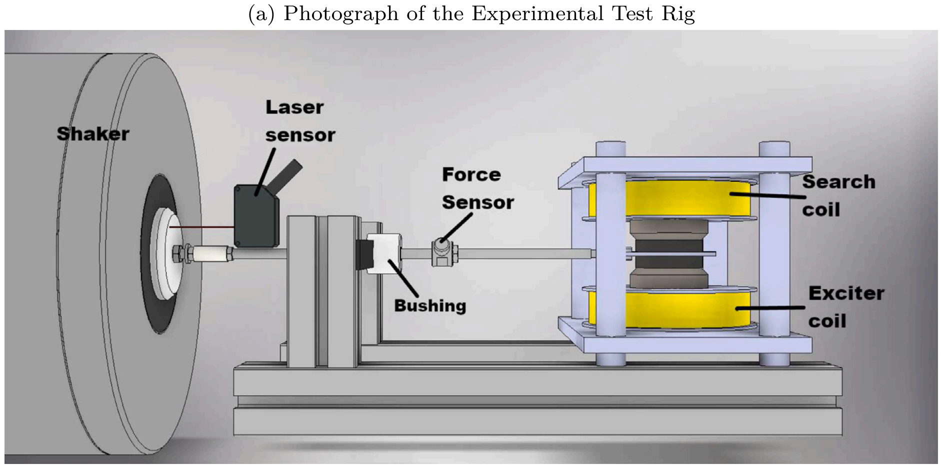

(b) Schematic Layout of the Main Components of the Test Rig

Fig. 7. Experimental test rig.

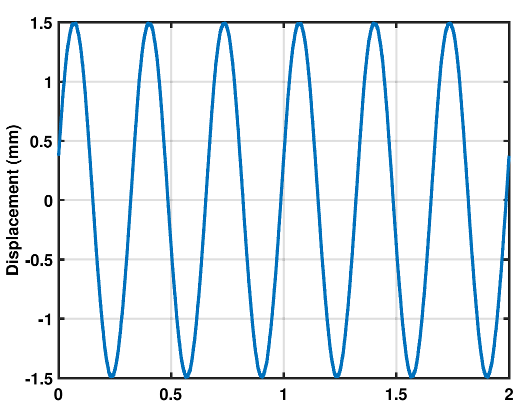

Fig. 8. Measured motion.

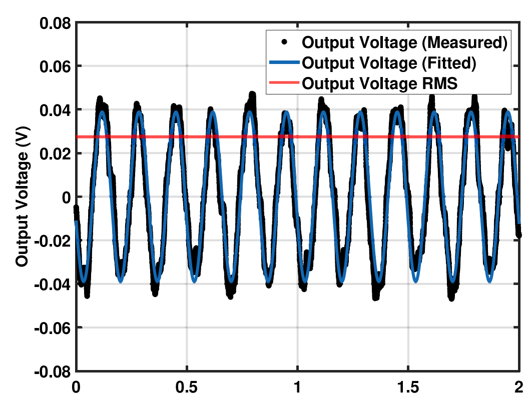

Fig. 9. Output voltage.

obtained by applying a magnetic field during their production to obtain anisotropic characteristics. As sustained from several works in literature, with the increase of the filling factor there is a reduction of the anisotropy degree, with a consequent decrease of the MR effect. In fact, a loss of anisotropy at the microscopic level is observed for specimens with a percentage of iron particles greater than 33% (Boczkowska et al., 2009, 2007). For this reason, the behavior expected from comparing these two specimens is that the 25% one should exert a higher output voltage level.

Indeed, as noticeable from Fig. 12(a), the tested specimens show an opposite behavior in which the 40% iron percentage MRE presents better properties. In particular, it shows a higher value of saturation of the magnetic field, indicated by the vertical red line and higher values of output voltage amplitude.

The same performance obtained for a sinusoidal displacement of 0.5 mm is obtained also for the displacement of 1.0 mm of amplitude, as illustrated in Fig. 12(b). Specifically, for low magnetic fields both specimens show almost the same level of output voltage whereas for

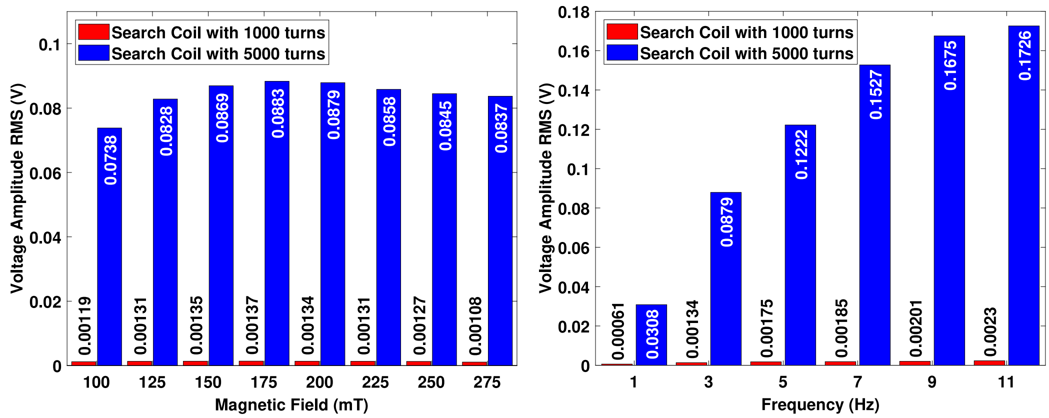

(a) Fixed 3 Hz - Different Magnetic Fields (b) Fixed 200 mT - Different Frequencies

Fig. 10. Search coil comparison.

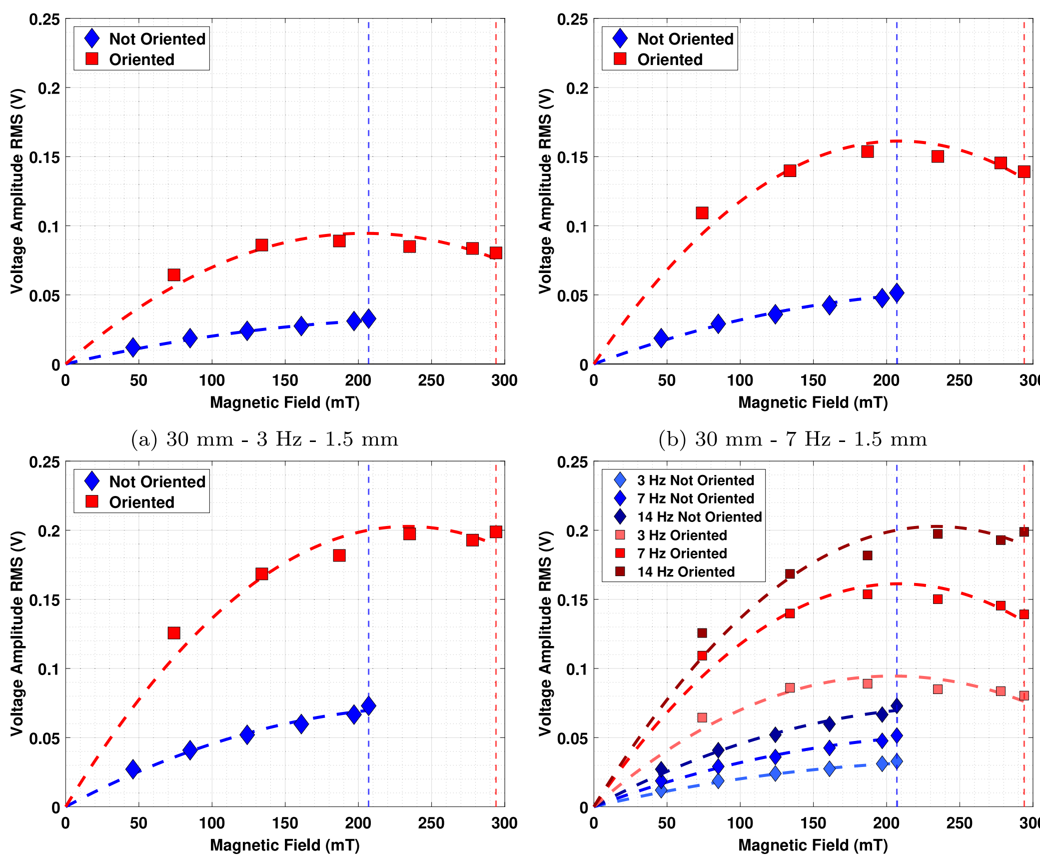

(c) 30 mm - 14 Hz - 1.5 mm (d) Frequencies Comparison - 30 mm - 1.5 mm

Fig. 11. Oriented VS Not Oriented — Vertical dashed lines represent the saturation values of the magnetic field.

magnetic field values higher than 200 mT the MRE with 40% of iron particles exhibits higher output voltages.

Finally, for the tests for an imposed displacement of 1.5 mm, shown in Fig. 12(c), an interesting trend reversal can be seen: for magnetic field values lower than approximately 400 mT the specimen with a lower percentage of particles reacts with a higher output voltage, for higher values, however, the opposite happens.

To summarize, it turns out that for small displacements amplitude, the specimen with 40% of iron shows better properties with a more marked inverse MR effect, a result in contrast with the reduced anisotropy of the specimen. For large displacements amplitude, the other specimen, with 25% of particles, generally considered as the optimal value for the creation of this type of specimens, shows higher values of the output voltage for small values of the magnetic field. From such experimental evidence, it would be possible to create different types of elastomers taking into account the amplitudes of the displacements, or vibrations, to which they would be subjected in order to obtain the highest output voltage value depending on the conditions of use.

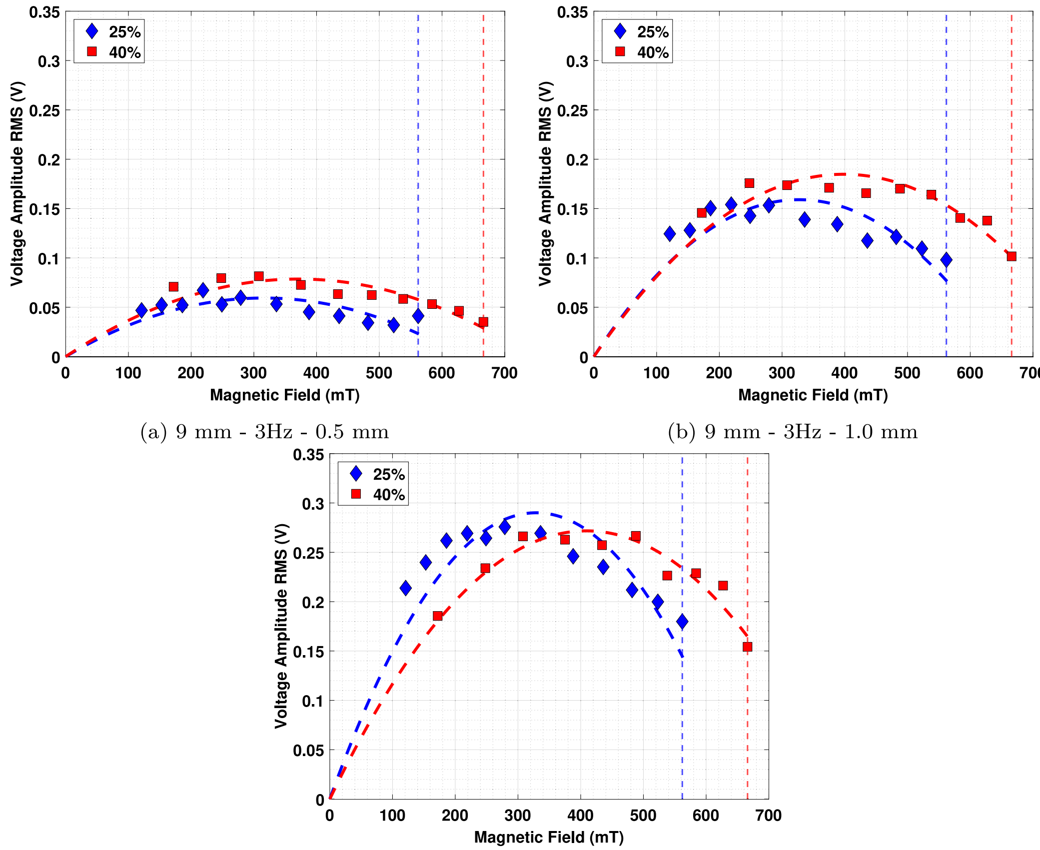

(a) 9 mm - 3Hz - 0.5 mm

(b) 9 mm - 3Hz - 1.0 mm

(c) 9 mm - 3Hz - 1.5 mm

Fig. 12. CIP percentage — 25% VS 40%.

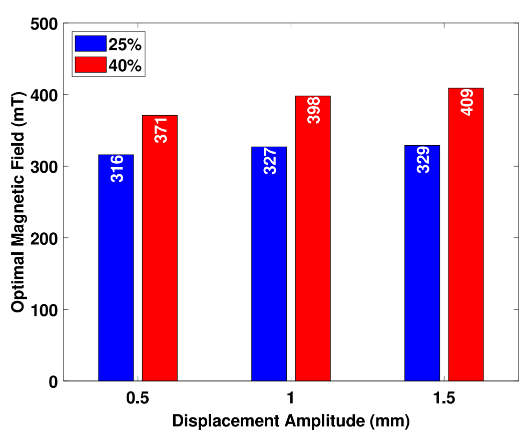

Fig. 13. Optimal magnetic field - 25% VS 40% - 9 mm - 3 Hz.

Finally, by exploiting the quadratic functions used to fit the experimental points, it was possible to define the magnetic field values corresponding to the maximum obtainable output voltage on the search coil. This magnetic field value will be indicated as the optimal magnetic field, also in the following sections. As it is reported in Fig. 13, the 25% specimen shows lower values of the optimal field if compared with the 40% specimen. In addition, both samples show a slightly increasing trend of the optimal magnetic field as the amplitude of the displacements increases.

3.5. Optimal magnetic field

In order to extend the validity of the considerations made in the previous section, a dedicated analysis is carried out to confirm the existence of an optimal magnetic field. In particular, several tests are performed on the 30 mm specimen, varying the supply current and the displacement amplitude. In Fig. 14(a) it is possible to highlight how for each displacement amplitude there is a maximum in the output voltage amplitude.

To investigate and visualize this phenomenon, a further comparison on the same data has been carried out, using as a reference the strain percentage, as shown in Fig. 14(b). The strain percentage $\epsilon_{\%}$ is evaluated as in Eq. (6),

$$\epsilon_{\%} = \frac{s}{H}100 \tag{6}$$

in which s represents the displacement amplitude and H the height of the specimen considered. The last figure confirms the existence of an optimum magnetic field, which in the case of the 30 mm high oriented specimen is approximately 235 mT.

It is important to underline that an optimal magnetic field is not observable for the specimen of the same height but not oriented, as can be deduced from Fig. 14(c). In this case, an increase in output voltage is observed as the magnetic field increases until its saturation, without observing any trend reversal, unlike the case previously described. This result confirms the substantially different behavior between the not-oriented and oriented specimens, further highlighting the latter's advantages: it allows higher output voltages in correspondence with magnetic fields lower than the saturation field.

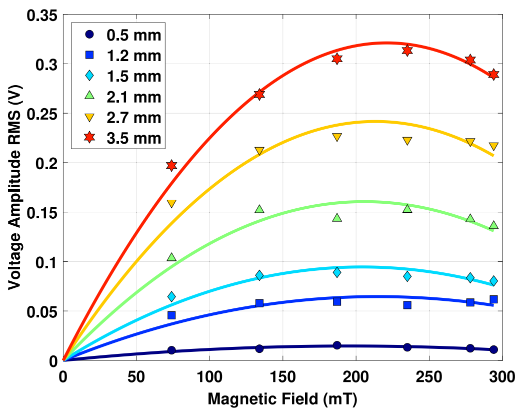

(a) Voltage VS Magnetic Field - 30 mm - Oriented - 3 Hz - Different Amplitudes

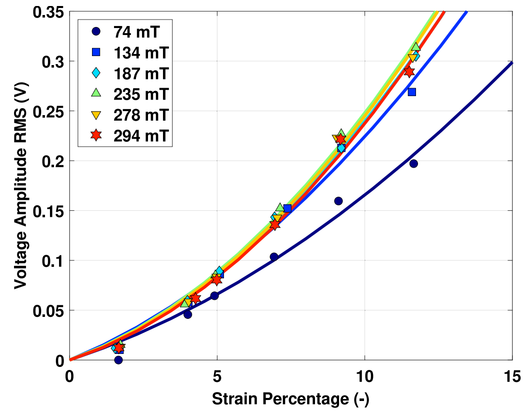

(b) Voltage VS Strain Percentage - 30 mm - Oriented - 3 Hz

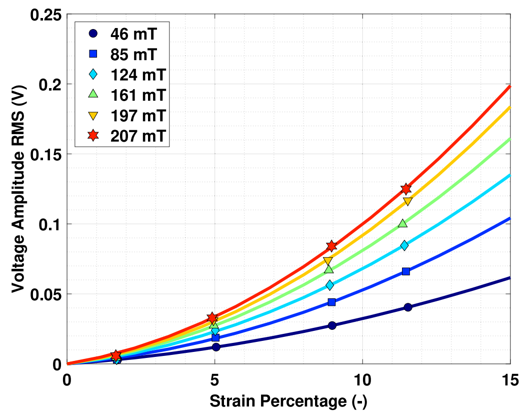

(c) Voltage VS Strain Percentage - 30 mm - Not Oriented - 3 Hz

Fig. 14. Optimal magnetic field.

3.6. Height dependence: 9 mm vs 30 mm

Thanks to the realization of specimens of different heights, 9 and 30 mm, it has been also possible to investigate the geometric influence on the inverse magnetorheological effect. To realize a proper comparison, the two geometries were compared both with the same displacement and with the same deformation. Starting from the comparison with equal displacement amplitude, the two specimens were compared for two displacement amplitudes of 0.5 mm and 1.0 mm, shown respectively in Figs. 15(a) and 15(b). As expected, the two graphs show that the 9 mm high specimen is able to generate higher output voltages for any magnetic field, if compared to the 30 mm high specimen. As already observed in the previous sections, in the case of the lower specimen the magnetic field saturates for higher values.

On the contrary, if we compare the specimens at the same strain percentage, as shown in Fig. 15(c) for a strain percentage value of 5% and in Fig. 15(d) for a strain percentage value of 11%, the behavior of the two specimens is reversed compared to the previous case, with the 30 mm specimen able to generate higher output voltages. These considerations provide a further evaluation parameter for the choice of the height of the elastomer specimen depending on the context in which it is to be used and for which the amplitudes of the displacements or deformations could be known a priori.

3.7. Frequency dependence

To conclude the presentation of the experimental evidence that emerged during the testing campaign, the variation of the inverse magnetorheological effect of the specimens by varying the frequency of the imposed displacement is highlighted. Referring to the 30 mm high oriented specimen, amplitude displacements of 1.5 mm were imposed as the frequency varied, starting from 1 Hz and increasing it by 2 Hz, up to 13 Hz. In this way, by varying the frequency of the displacement and the supply current (i.e. the magnetic field inside the specimen), it was possible to obtain the graph in Fig. 16. Avoiding repeating the considerations already discussed in the previous sections, it is important to note that the output voltage increases as the frequency of the displacement increases. The arrangement of the curves suggests a possible saturation frequency, beyond which it should not be possible to obtain higher output voltage values or a reversal of the trend of the curves could be observed, as already observed for the optimum field. This trend is suggested by the less than proportional increase in output voltage as frequency increases. During the test campaign carried out, higher frequencies were not reached, but this further exploration will be the subject of future experiments in order to confirm the hypotheses just formulated.

4. Conclusions

This article presents an experimental investigation to study the variation of MREs inverse effect properties. The test matrix, the fabrication of specimens with different characteristics, and the definition of the optimal experimental setup were designed to enable the comparison of specimen pairs with varying properties and to highlight trends and functional dependencies. The main findings highlighted during the campaign can be summarized as follows:

- According to the literature, the anisotropic specimen presents a greater MR inverse effect than the isotropic specimen, making the latter inefficient from an energy conversion point of view;

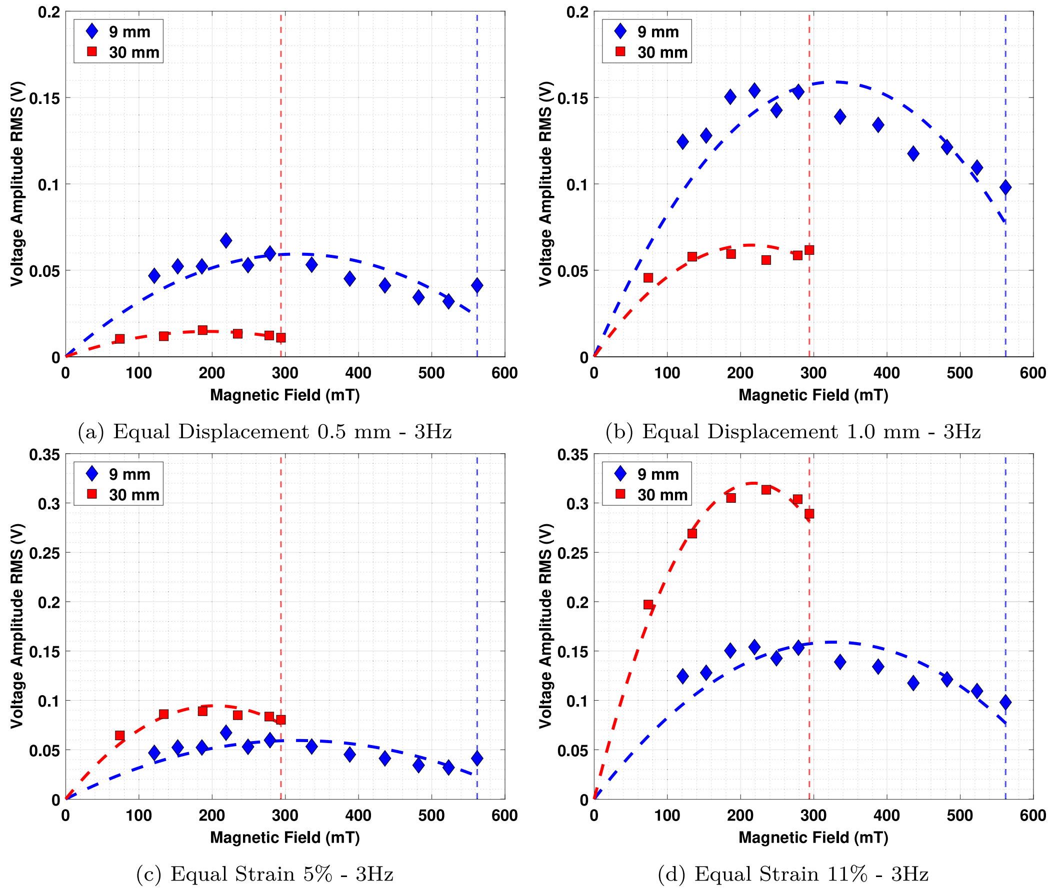

(a) Equal Displacement 0.5 mm - 3Hz

(b) Equal Displacement 1.0 mm - 3Hz

(c) Equal Strain 5% - 3Hz

(d) Equal Strain 11% - 3Hz

Fig. 15. Specimens' geometry - 9 mm VS 30 mm.

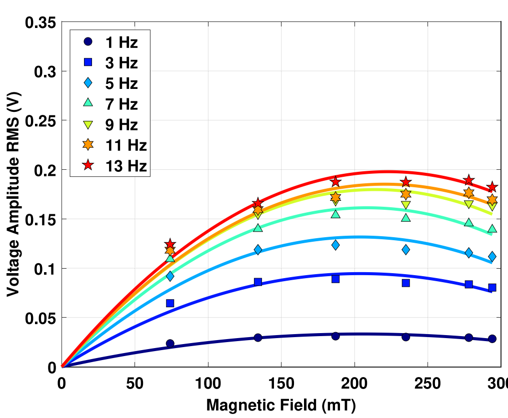

Fig. 16. Frequency dependence - 30 mm - Oriented - 1.5 mm.

- Increasing CIP does not always translate into increased energy conversion efficiency. In particular, for low displacement amplitudes, a higher MR inverse effect for higher CIP percentages is observable. The trends are even more complex for larger displacement amplitudes: for low magnetic field values, the specimen with a lower CIP percentage shows higher performance and vice versa.
- It was possible to identify an optimal magnetic field for the oriented samples, lower than the saturation magnetic field. This information allows to further optimize the choice of the permanent magnet to be used for energy harvesting applications.
- The height of the specimen plays a fundamental role in optimizing the energy conversion depending on whether a specific deformation or displacement can be imposed on the specimen. Knowing this information a priori gives the possibility to develop the most suitable MRE for the specific case.
- Finally, a frequency dependence of the induced specimen displacement was highlighted, whereby the output voltage increases with frequency less than proportionally.

These findings represent a crucial result in understanding the main physical dependencies that influence the behavior of MREs in the context of their potential for energy harvesting. Certainly, through more extensive experimental campaigns, it would be possible to further highlight the limitations of these materials, revealing their saturation with respect to certain factors already partially explored in this work (by increasing the range of explored frequencies and creating additional samples with different CIP percentages and various heights); moreover, new effects such as temperature dependence could be investigated. Understanding these dependencies constitutes a fundamental preliminary step toward building a phenomenological model aimed not only at determining the variable stiffness of these materials but also at evaluating the recoverable energy for energy harvesting applications. Among future projects, there is also the development of a complete sensor application case study, using the MREs as a displacement transducer or as a vibration monitoring system, with particular attention to the design of the output electrical system for effective energy storage.

CRediT authorship contribution statement

Guido Napolitano Dell'Annunziata: Writing – review & editing, Writing – original draft, Visualization, Validation, Software, Methodology, Investigation, Data curation. **Renato Brancati:** Writing – review

& editing, Writing – original draft, Supervision, Resources, Project administration, Formal analysis, Conceptualization. **Giandomenico Di Massa:** Resources, Investigation, Formal analysis, Data curation. **Andrea Genovese:** Writing – review & editing, Writing – original draft, Validation, Supervision, Software, Project administration, Methodology, Conceptualization.

Declaration of competing interest

The authors declare that they have no known competing financial interests or personal relationships that could have appeared to influence the work reported in this paper.

Data availability

Data will be made available on request.

References

Ahmad, M.M., Khan, N.M., Khan, F.U., 2021. Review of frequency up-conversion vibration energy harvesters using impact and plucking mechanism. Int. J. Energy Res. 45 (11), 15609–15645.

Bahl, S., Nagar, H., Singh, I., Sehgal, S., 2020. Smart materials types, properties and applications: A review. Mater. Today: Proc. 28, 1302–1306.

Bellelli, A., Vairo, A., Spaggiari, A., 2025. Design and characterization of a magnetorheological elastomer linear actuator for low-frequency applications. J. Braz. Soc. Mech. Sci. Eng. 47 (3), 137.

Boczkowska, A., Awietjan, S., Wejrzanowski, T., Kurzydłowski, K., 2009. Image analysis of the microstructure of magnetorheological elastomers. J. Mater. Sci. 44, 3135–3140.

Boczkowska, A., Awietjan, S.F., Wroblewski, R., 2007. Microstructure–property relationships of urethane magnetorheological elastomers. Smart Mater. Struct. 16 (5), 1924.

Brancati, R., Di Massa, G., Genovese, A., 2023. Experimental investigation to enhance performances of MRE in energy harvesting. In: International Workshop IFToMM for Sustainable Development Goals. Springer, pp. 3–10.

Cansiz, M., Altinel, D., Kurt, G.K., 2019. Efficiency in RF energy harvesting systems: A comprehensive review. Energy 174, 292–309.

Carlson, E.J., Strunz, K., Otis, B.P., 2010. A 20 mV input boost converter with efficient digital control for thermoelectric energy harvesting. IEEE J. Solid-State Circuits 45 (4), 741–750.

Costi, L., Georgopoulou, A., Mondal, S., Iida, F., Clemens, F., 2024. 3D printable self-sensing magnetorheological elastomer. Macromol. Mater. Eng. 309 (2), 2300294.

Deng, Z., Dapino, M.J., 2017. Review of magnetostrictive vibration energy harvesters. Smart Mater. Struct. 26 (10), 103001. http://dx.doi.org/10.1088/1361-665X/aa8347.

Díez, A.G., Tubio, C.R., Etxebarria, J.G., Lanceros-Mendez, S., 2021. Magnetorheological elastomer-based materials and devices: state of the art and future perspectives. Adv. Eng. Mater. 23 (6), 2100240.

Diguet, G., Sebald, G., Nakano, M., Lallart, M., Cavaillé, J.-Y., 2020a. Analysis of magneto rheological elastomers for energy harvesting systems. Int. J. Appl. Electromagn. Mech. 64 (1–4), 439–446.

Diguet, G., Sebald, G., Nakano, M., Lallart, M., Cavaillé, J.-Y., 2020b. Optimization of magneto-rheological elastomers for energy harvesting applications. Smart Mater. Struct. 29 (7), 075017.

Ding, W., Wang, L., Chen, Z., Ao, H., Yan, H., 2024. An adaptive elastic support seat-based magnetorheological elastomer for human body vibration reduction. Materials 17 (13), 3330.

of the IEEE, S.C., 1991. IEEE standard on magnetostrictive materials: Piezomagnetic nomenclature. p. 1. http://dx.doi.org/10.1109/IEEESTD.1991.101048, IEEE Std 319-1990.

Jaafar, M., Mustapha, F., Mustapha, M., 2021. Review of current research progress related to magnetorheological elastomer material. J. Mater. Res. Technol. 15, 5010–5045.

Jolly, M.R., Carlson, J.D., Muñoz, B.C., Bullions, T.A., 1996. The magnetoviscoelastic response of elastomer composites consisting of ferrous particles embedded in a polymer matrix. J. Intell. Mater. Syst. Struct. 7 (6), 613–622.

Lallart, M., Sebald, G., Diguet, G., Cavaille, J.-Y., Nakano, M., 2017. Anisotropic magnetorheological elastomers for mechanical to electrical energy conversion. J. Appl. Phys. 122 (10).

Li, Z., Yin, W., Li, Z., 2025. Research on intelligent vibration damping base of washing machine based on a stiffness-variable magnetorheological elastomer. Sound & Vib. 59 (1), 2036–2036.

Liang, H., Hao, G., Olszewski, O.Z., 2021. A review on vibration-based piezoelectric energy harvesting from the aspect of compliant mechanisms. Sensors Actuators A: Phys. 331, 112743.

Lin, Y., Wen, G., Liu, C., He, J., Liu, J., 2025. A magnetorheological elastomer-based hybrid vibration isolation system with semi-active control and quasi-zero stiffness performance. Int. J. Non-Linear Mech. 174, 105063.

Mahapatra, S.D., Mohapatra, P.C., Aria, A.I., Christie, G., Mishra, Y.K., Hofmann, S., Thakur, V.K., 2021. Piezoelectric materials for energy harvesting and sensing applications: roadmap for future smart materials. Adv. Sci. 8 (17), 2100864.

Nicolay, P., Schlögl, S., Thaler, S.M., Humbert, C., Filipitsch, B., 2023. Smart materials for green (er) cities, a short review. Appl. Sci. 13 (16), 9289.

Nugroho, K.C., 2024. Influence of carbonyl iron particles on the structural and mechanical performance of magnetorheological elastomers. Multidiscip. Innov. Res. Appl. Eng. 1 (1), 21–32.

Schwartz, M., 2002. Encyclopedia of smart materials, 2 volume set.

Sebald, G., Nakano, M., Lallart, M., Tian, T., Diguet, G., Cavaille, J.-Y., 2017. Energy conversion in magneto-rheological elastomers. Sci. Technol. Adv. Materials 18 (1), 766–778.

Šimić, D., Lang, A., Klüppel, M., 2023. Inductive and magnetorheological properties of soft and hard magnetic fillers in elastomers. Smart Mater. Struct. 32 (12), 125016.

Sobczyk, M., Wiesenhütter, S., Noennig, J.R., Wallmersperger, T., 2022. Smart materials in architecture for actuator and sensor applications: A review. J. Intell. Mater. Syst. Struct. 33 (3), 379–399.

Trinh, V.-L., Chung, C.-K., 2023. Advances in triboelectric nanogenerators for sustainable and renewable energy: Working mechanism, tribo-surface structure, energy storage-collection system, and applications. Processes 11 (9), 2796.

Wang, X., Gordaninejad, F., Calgar, M., Liu, Y., Sutrisno, J., Fuchs, A., 2009. Sensing behavior of magnetorheological elastomers. J. Mech. Des. 131 (9), 091004.

Yang, Z., Erturk, A., Zu, J., 2017. On the efficiency of piezoelectric energy harvesters. Extrem. Mech. Lett. 15, 26–37.

Zhang, C., 2023. Comparison of triboelectric nanogenerator and electromagnetic generator. In: Handbook of Triboelectric Nanogenerators. Springer, pp. 505–538.

Zhao, J., Zhao, Y., Shen, F., Li, X., Yin, L., 2024. Experimental and numerical study on seismic behavior of high energy-consuming resilient concrete shear walls reinforced by CFRP bars and magnetorheological dampers. In: Structures, vol. 68, Elsevier, 107210.

Zheng, Y., Tang, N., Omar, R., Hu, Z., Duong, T., Wang, J., Wu, W., Haick, H., 2021. Smart materials enabled with artificial intelligence for healthcare wearables. Adv. Funct. Mater. 31 (51), 2105482.